A Tutorial on Beam Loss Monitoring

Robert E. Shafer

TechSource, Inc.
Santa Fe, NM

Abstract. The beam loss monitoring system is one of the two most widely distributed beam diagnostic systems at most particle accelerator facilities. This tutorial reviews the characteristics of the ionizing radiation from beam losses, and the properties of beam loss radiation detectors.

INTRODUCTION

The beam loss monitoring system is one of the two most widely distributed beam diagnostic systems at most particle accelerator facilities. In addition to being a beam-tuning device, beam loss monitors (BLMs) are the front-line devices for protecting the beam line components from damage due to beam loss. In addition, the BLMs monitor losses that lead to long-term activation and radiation damage, as well as provide alarms when the radiation from beam losses may lead to excessive radiation levels outside the radiation enclosures.

The Effects of Ionizing Radiation

The effects of ionizing radiation can be categorized in the following table.

Material damage	overheating, thermal stress, radiation damage.
Cryogenic systems	excessive heat load, magnet quenching.
Optics	darkening (optical transmission).
Solid-state electronics	single event upset, long-term damage (dislocations).
Activation	personnel hazard (exposure).
Prompt radiation	backgrounds in experiments.
	personnel hazard (neutrons).

Sources of Ionizing Radiation

Ionizing radiation can come from both beam and non-beam sources:

- Beam halo
- Residual gas stripping (H- beams)
- Focus and steering errors
- Foreign objects in the beam
- X-rays from rf cavities
- Residual gas scattering
- Magnetic stripping (H- beams)
- Intercepting beam diagnostics
- Synchrotron radiation

CP648, *Beam Instrumentation Workshop 2002: Tenth Workshop,* edited by G. A. Smith and T. Russo

Types of Ionizing Radiation

Types of ionizing radiation from high-energy particle beams include protons, electrons, pions, muons, gammas (including x-rays), and neutrons. Lost protons, if they are over a few GeV, will produce secondaries via hadronic showers, which includes pions, neutrons, and muons. Pi-zeros produce high-energy gammas. Lost electrons produce electromagnetic showers via bremsstrahlung. Gamma rays produced in electromagnetic showers convert back to electrons via Compton scattering and pair production.

DETECTION OF IONIZING RADIATION

Eventually, the primary mechanism by which a beam loss monitor detects beam loss is by ionization or by fluorescence. Both ionization and fluorescence represent a transfer of energy from the incoming charged particle to the *atomic electrons*. Interactions between the incident particle and *nuclei* are far less likely, and usually transfer momentum, rather than energy, resulting in multiple Coulomb scattering and beam divergence growth.

Energy loss of incident charged particles scattering on atomic electrons is described by the Bethe-Bloch equation, found in most textbooks on nuclear and particle physics.

$$dE/dx = -\frac{4\pi e^4 N_A}{\beta^2 mc^2}\frac{Z}{A}\left[\ln\left(\frac{2\beta^2 mc^2}{I}\right) - \ln\left(1-\beta^2\right) - \beta^2\right] \text{ eV per gram/cm}^2 \quad (1)$$

where mc^2 is the electron rest mass, and β refers to the incident charged particle velocity, with charge z=1. A complete discussion of this equation can be found in the relevant textbooks. A plot of dE/dx for protons in aluminum and lead are shown in Figure 1. A complete set of dE/dx and range tables for protons in most elements can be found at the NIST website[1].

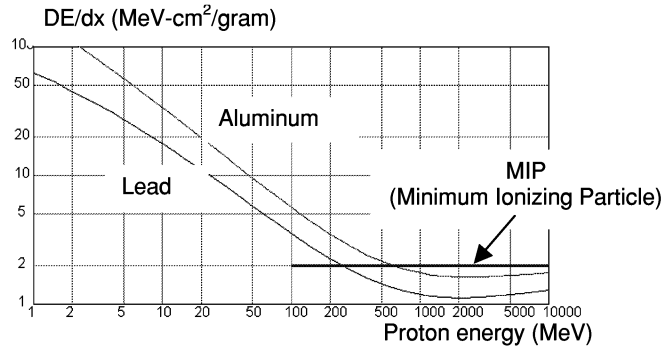

Figure 1. Plot of energy loss dE/dx vs. energy of incident proton.

The minimum in dE/dx, generally between 1 and 5 GeV for protons, is between 1 and 2 MeV-cm^2/gram. It is convenient to define a mythical Minimum Ionizing

Particle (*MIP*) as a particle that has an energy loss of 2 MeV-cm^2/gram (shown as a line in Figure 1).

Using the definition of a rad of radiation dose as 100 ergs per gram leads to another definition, in terms of *MIP*s.

$$1\,rad = \frac{100\,ergs}{gram} \cdot \frac{MeV}{1.6 \cdot 10^{-6}\,ergs} \cdot \frac{MIP \cdot gram}{2\,MeV \cdot cm^2} = 3.1 \cdot 10^7\ MIPs\ per\ cm^2 \qquad (2)$$

So now we can describe the rad response of a beam loss monitor in terms of either energy deposition (100 ergs/gram), or in terms of a charged particle flux ($3.1 \cdot 10^7$ *MIP*s/cm^2).

Radiation Detection Methods

The most common method for detecting ionizing radiation is to observe the interaction of charged particles with the atomic electrons in the detector, by measuring the ionization charge (ionization chambers), the fluorescence (phototube-scintillator combinations), or the secondary emission current (SEM chambers). Other methods of detecting the ionizing radiation include measuring Cerenkov light (from relativistic charged particles) or Compton electrons (from high energy gammas). Other detection methods (e.g., Smith Purcell radiation) have not been found to be useful.

Considerations in selecting a beam loss monitor

There are many factors that must be considered in selecting a beam loss monitor design. Some relate to the type of radiation, some relate to the expected dose rates and peak pulsed doses, and some relate to other factors such as reliability, physical space, calibration issues, cost, etc. Another consideration is whether to use an integrating type, whose output is measured in Coulombs per rad, or a pulse type detector, whose output is measured in counts per rad. A few factors are listed below.

Detector output signal (current-integrating or pulse-type outputs)
Sensitivity (Coulombs or pulses per rad)
Detector dynamic range (rads per sec and instantaneous rad doses)
Saturation characteristics for high radiation doses
Sensitivity to backgrounds (e.g., RF cavity x-rays, synchrotron radiation)
Sensitivity to magnetic fields
Sensitivity to high voltage drift (e.g., photomultipliers)
Uniformity of calibration (unit to unit)
RAMI analysis (reliability, availability, maintainability, inspectability)
On-line system testability
Periodic calibration requirements
Radiation hardness of materials used in construction
Bandwidth (time resolution)
Robustness (suitability for use in an accelerator enclosure environment)
Physical size
Cost

BEAM LOSS MONITORS USING IONIZATION DETECTION

When a charged particle passes through a gas, the gas is ionized, producing ion electron pairs. The amount of energy loss in creating an ion-electron pair is called the ionization constant. The following list shows the ionization constant for some common gases[2].

Gas	Ionization constant	Gas	Ionization Constant
Air	34 eV	hydrogen	36 eV
Helium	41	nitrogen	35
Neon	36	argon	26
Krypton	23	xenon	21

We can use these numbers to estimate the ionization yield per MIP in a cm of argon gas at STP:

$$N = \frac{1\,ion\ pair}{26\,eV}\frac{2\cdot 10^{6}\,eV\cdot cm^{2}}{MIP\ gram}\frac{40\,grams}{22{,}414\,cm^{3}} = \frac{140\,ion\ pairs}{cm}\ per\ MIP \qquad (3)$$

We can also estimate the number of Coulombs per rad in argon:

$$N = \frac{140\,ion\ pairs}{MIP\,cm}\cdot\frac{3.1\cdot 10^{7}\,MIPs}{cm^{2}\,rad}\cdot\frac{1.6\cdot 10^{-19}\,C}{ion\ pair} = 700\ pC/cm^{3}\ per\ rad \qquad (4)$$

We can also make the same estimate more directly from the definition of a rad:

$$1\,rad = \frac{100\,ergs}{gram}\frac{1\,eV}{1.6\cdot 10^{-12}\,ergs}\frac{1\,ion\ pair}{26\,eV}\frac{1.6\cdot 10^{-19}\,C}{ion\ pair}\frac{40\,grams}{22{,}414\,cm^{3}} = 700\,pC/cm^{3} \qquad (5)$$

We can also calculate the cross section for creating an ion pair in argon, to compare to nuclear interaction rates:

$$\sigma = \frac{1\,pair}{26\,eV}\frac{2\cdot 10^{6}\,eV\,cm^{2}}{gram}\frac{40\,grams}{6\cdot 10^{23}\,atoms} = 5\cdot 10^{-18}\,cm^{2}\ per\ atom \qquad (6)$$

This is roughly 6 orders of magnitude larger than typical nuclear cross sections.

Because we will also discuss solid-state "ionization chambers" (silicon PIN diodes), the number of electron-hole pairs per cm in silicon per MIP is

$$N = \frac{1\,pair}{3.6\,eV}\frac{2\cdot 10^{6}\,eV\,cm^{2}}{MIP\ gram}\frac{2.3\,grams}{cm^{3}} = 1.4\cdot 10^{6}\,\frac{electron-hole\ pairs}{cm}\ per\ MIP \qquad (7)$$

So the charge production in solid-state ion chambers is much larger than in gas ion chambers.

Finally, we calculate the response of a 100 cm^2, 21-foil secondary-electron-emission monitor (SEM) to MIPs:

$$1\,rad = \frac{3.1\cdot 10^{7}\,MIPs}{cm^{2}}\cdot 100\,cm^{2}\cdot\frac{0.01\,electrons}{surface}\cdot 20\,surfaces\cdot\frac{1.6\cdot 10^{-19}\,C}{electron} = 100\,pC \qquad (8)$$

So a SEM detector is a very inefficient beam loss monitor.

Gas Ionization Chambers

We first review the properties of ionization chambers in general. At very low applied voltages, the collection of ion-electron pairs is inefficient, because of recombination before the charges reach the electrodes. As the voltage is increased, the collection efficiency usually reaches 100%, unless the density of ions and electrons is too large or the recombination rate is too high. As the voltage is raised further in cylindrical chambers with the electrons collected on the inner conductor (the preferred polarity) gas multiplication begins. There are two mechanisms for multiplication. The first is gas fluorescence near the anode producing uv light which in turn produces photoelectrons on the cathode. The second is ionization of the gas near the anode producing more ion-electron pairs. This is referred to as the proportional mode. In this mode, the multiplication is very dependent on the applied voltage, unlike the ionization chamber that has multiplication of 1.

Finally, as the voltage is raised further, the gas actually breaks down, discharging the voltage across the chamber. This is called the Geiger mode. In this case, the amplitude of the pulse is independent of the initial ionization. Because the tube voltage is discharged, the tube is "paralyzed" for 10's or 100"s of microseconds until the voltage recharges.

In cylindrical ion chambers with the inner conductor having positive polarity, more than 50% of the external signal is due to the motion of the electrons (or negative ions), and less than 50% due to motion of the positive ions. For a cylindrical ion chamber with a 6:1 diameter ratio, 75% of the total external signal is due to the motion of the electrons. This is because most of the image charges for both ions and electrons are initially on the outer electrode. The current in the external circuit is due to the motion of these image charges from one electrode to the other, as the internal charges drift to the electrodes. In the case of proportional and Geiger tubes, additional charge carriers are created near the anode, and most of the external signals are thus due to positive ions rather than to electrons.

The preference for having positive polarity on the center electrode arises from the relative drift velocities of electrons and ions. At 1 atm, electron drift velocities at 1000 V/cm are of the order of 1 cm per μs (depending on the specific gas), while for positive ions, it is of the order of 1 cm/ms. Thus when the center electrode is positive, the dominant signal is produced by the high mobility electrons, providing a dominant fast external signal, while the slow moving ions produce a relatively small external signal.

Because the number of ion pairs created per incident MIP is small (about 140 pairs per cm in argon gas at 1 atm), gas ion chambers are always used in the current-integrating (charge) mode. Typically, the calibration ranges from about 50 to 500 nanoCoulombs per rad.

The ion chamber dynamic range is limited by leakage currents at the low end, and by charge recombination at the high end[3]. Good guard-ring design will limit leakage currents to 1 pA or less. In argon ion chambers, recombination is less because the free electron does not attach to neutral ions to form negative ions. In cases where the recombination is very small, the positive ion space-charge density can inhibit ion collection, and have a similar effect[4]. The dynamic range of the FNAL chamber

discussed below is limited to about 100 rads/sec (7 μA) on the high end, thus giving a dynamic range of over 10^6 to 1. Maintaining this dynamic range in the front-end electronics at these low currents is difficult.

Unlike pulse-counting beam loss monitors, current-integrating ion chambers have a very high instantaneous dose limit. Very roughly, the instantaneous dose limit is the dose rate limit (e.g., 100 rads/sec mentioned above) times the positive ion collection time (typically about 1 msec), or 0.1 rads. A pulse-type detector with a calibration of 1 Hz at 1 rad/hr would have to count at 360 MHz to measure a 0.1-rad pulse in 1 μsec.

The FNAL Argon Ionization Chamber

The FNAL argon ionization chamber[5] is an example of a conventional ion chamber developed for use around accelerators. It is a sealed-glass cylindrical ion chamber, with 10-cm long nickel electrodes, 3.81-cm outer electrode diameter and 0.635-cm inner electrode diameter. It is shown in Figure 2. The inner electrode is the anode (signal output), and the outer electrode is the cathode, biased at –2000 volts. Connections are at opposite ends of the sealed glass chamber, and a guard ring is painted on the outside of the glass to minimize end-to-end leakage currents. Its active volume is about 110 cm^3, and it is filled with argon gas at 725 mm Hg. Argon gas was chosen because the electron attachment rate to form negative ions is very small, and the electron drift velocity is about 0.5 cm/μs, thus giving a large prompt signal. Its calibration, using Eqn (5), is about 70 nC per rad. Because the chamber is sealed and there are no organic materials inside, it requires no gas replacement.

Figure 2. FNAL 110-cm^3 sealed-glass argon ionization chamber and its container.

Figure 3 shows a saturation curve for five identical ion chambers taken with a radioactive source. Note in particular that all chambers have the same output current, and that the saturation plateau ranges from about 200 volts to over 2000 volts. A beneficial characteristic of ion chambers is that the rad calibration is determined by geometry, and that the calibration is relatively independent of the applied voltage. This

Figure 3. Voltage-plateau curves for five identical modified FNAL argon ionization chambers (from Witkover and Gassner, this conference).

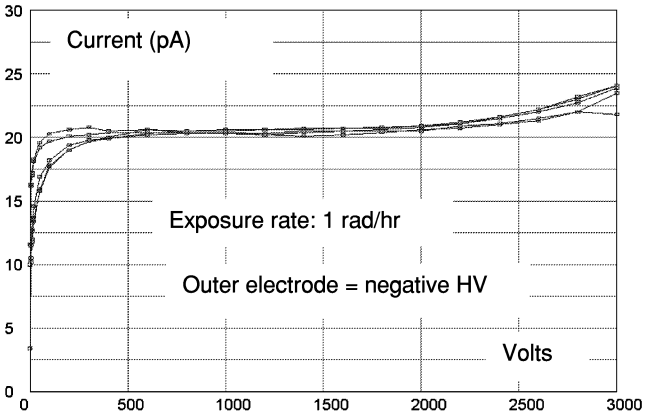

simplifies the system design in large installations, because the high voltage can be daisy-chained to many BLMs, and periodic calibrations are not required.

System readiness tests include pulsing the high voltage under computer control, and measuring the induced charge output. Because the inter-electrode capacitance is about 2 pF, a 2000-volt pulse induces about 4 nC of charge in the external circuit that can be digitized.

Figure 4 shows predicted charge-collection efficiency curves for the FNAL chamber at 1, 10, and 100 rads/sec. These curves are based on the theory of recombination in cylindrical ionization chambers[6]. This design was tested with an electron-linac pulsed radiation source up to about 1 rad instantaneous dose.

Charge collection fraction for 1,10, and 100 rads/sec dose rates vs. applied voltage, for the FNAL ionization chamber.

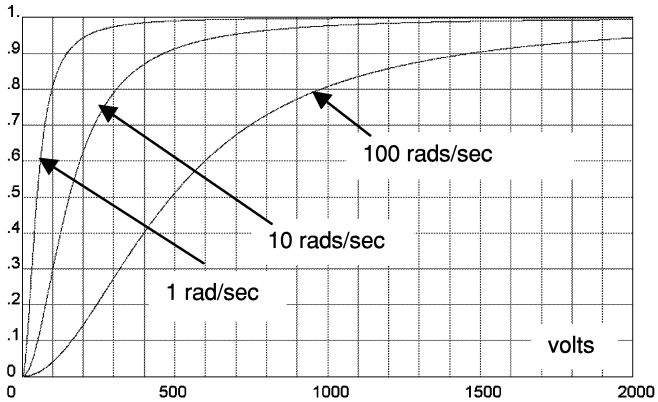

Figure 4. Predicted charge-collection efficiency for 3 dose rates vs. voltage.

The Spallation Neutron Source (SNS) beam loss at 1 GeV in the H- linac is expected to be about 1 watt/meter, which corresponds to an average dose rate of about 50 rads/hr at 30 cm. This is equivalent to about 0.25 rads/sec during the 60 Hz, 1-ms beam macropulses. Thus the FNAL argon ion chamber can monitor dose rates up to 400 times the nominal dose rate with less than about 6% recombination loss.

During commissioning of the SNS linac, an entire 600-ns, 1-GeV, millipulse could be lost at a point. The estimated rad dose at 30 cm is about 0.3 rads, which corresponds to a dose rate of about 500 krad/sec. Figure 5 shows plots of the predicted pulsed rad dose charge collection efficiency for 0.001, 0.01, and 0.1 rads vs. voltage for the FNAL ion chamber[6].

Charge collection fraction for 0.001. 0.01 and 0.1 rads instantaneous pulsed dose, for the FNAL ionization chamber.

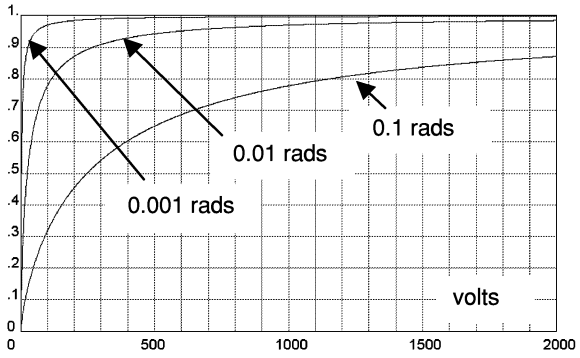

Figure 5. Predicted charge-collection efficiency for 3 pulsed doses vs. voltage.

Long Ion Chambers (PLICs)

Panofsky long ionization chambers (PLICs) have been in use at SLAC since 1966[7]. The original PLIC was 1.5" dia. Heliax cable, 2-km long, filled with Ar/CO_2 gas. The outer conductor was grounded and the inner conductor was +HV, and the output signal was ac-coupled. Because the electron beam pulse was very short (< 2 μs), the up-beam PLIC signal (pulses traveling in the opposite direction to the beam) could be used to determine the beam-loss point to a few meters. Many variations of this original design are now in use at SLAC.

Unlike conventional ion chamber designs, variations of the original PLIC design can be very fast, and can determine loss points by time-of-flight with roughly 1-meter resolution. In Figure 6, the pulse response is shown for two PLIC designs, both using a very fast gas, Ar/CF_4, with an electron drift velocity of about 12 cm/μs[8,9].

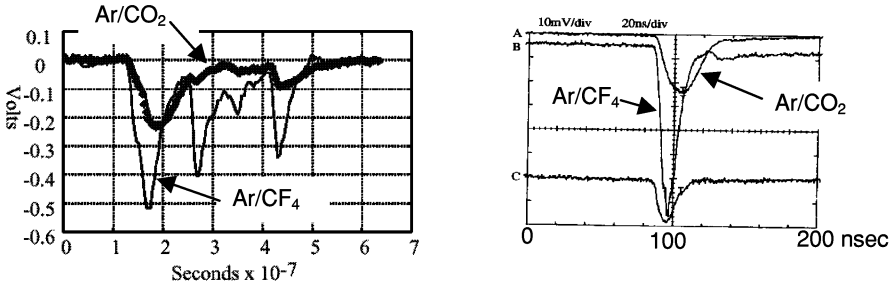

Figure 6. Fast Ar/CF_4 up-beam PLIC pulses from point losses at SLAC.

Solid State Ion Chambers (PIN Diodes)

Solid-state ionization chambers are usually reverse-biased silicon PIN diodes with frontal areas ranging from a few to 100 mm^2, and with depletion depths ranging from perhaps 100 to 300 μm. They can be used in either the current output mode or the pulsed output mode. We review the basic characteristics of two PIN diodes, the Siemens BPW 34 and the Hamamatsu S2662, used in some beam loss monitors.

Property	BPW 34	Hamamatsu S2662
Area	2.75 x 2.75 mm^2	7.5 x 20 mm^2
Depletion depth	~100 μm	~100 μm
Volume	0.75 mm^3	15 mm^3
Leakage current	~100 pA	~500 pA
Integrating mode		
Coulombs per rad	5 nC	100 nC
Rad equiv. of leakage current	70 rads/hr	20 rads/hr
Rad hardness (leakage current)	~1 Mrad	~1 Mrad
Pulse mode		
MIPs per rad	2.3E6	4.6E7
Max rads/sec (@ 10^7 counts/sec)	4 rads/sec	0.2 rads/sec
Rad hardness (spurious counts)	~100 Mrads	~100 Mrads

PIN Diode Pulse-Mode Coincidence Circuit BLM

In order to minimize the sensitivity to synchrotron radiation, two PIN diodes can be placed back-to-back, and the two pulse-output signals put into a coincidence circuit. Such a unit has been developed at DESY for use in the HERA tunnel which also has a 30-GeV electron ring[10]. The detector geometry is shown in Figure 7. Low energy photons will interact in only one PIN diode, while MIPs interact in both, producing a coincidence. The unit also has directional sensitivity. The whole unit measures about 69 mm by 34 mm by 18 mm. It is now commercially available[11].

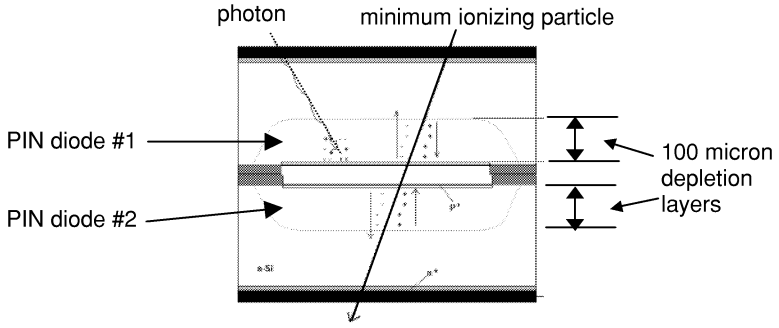

Figure 7. PIN diode coincidence circuit.

BEAM LOSS MONITORS USING LIGHT DETECTION

Detection of beam-induced light in scintillators or Cerenkov radiators represents the other most common method of monitoring beam losses. The scintillation process is also based on the Bethe-Bloch *dE*/*dx* equation. Some combinations, using the current-integrating mode, are:

Phototube	Radiator
Photomuliplier Tube	Organic scintillator (e.g., NE 102 or BC-400) Liquid scintillator (mineral oil based) Inorganic scintillators (e.g., CsI(Tl), BGO) Cerenkov radiator (e.g., fused silica) Bare PMT
Vacuum Photodiode	Scintillators as per above list Cerenkov radiators as per above list

Scintillation constants of some organic and organic scintillator materials are listed below[12].

Scintillator	Scintillation constant
Inorganic	
NaI(Tl)	26 eV energy loss per emitted photon
CsI(Tl)	15
BGO ($Bi_4Ge_3O_{12}$)	122
$CdWO_4$	67
CsI (unacivated)	500
Ce-activated Li glass	300
Organic	
Anthracene	60
NE-102A	100
BC-400	90
BC-517P (mineral oil)	250
Gas	
Nitrogen	1250

A useful feature of scintillators is the very fast risetime (a few to 100's of ns). Rad hardness varies from a few krads (e.g., NaI(Tl)) to about 100 Mrad (BGO, aka $Bi_4Ge_3O_{12}$). We examine two scintillator-based beam loss monitors.

The LAMPF "Paint Can" Beam Loss Monitor

The LAMPF "paint can" beam loss monitor is a 1-pint paint can filled with mineral-oil-based liquid scintillator. It uses a side-window photomultiplier (NE-4552) mounted inside the can, along with the voltage-divider resistor chain and a calibration

lamp. It operates on negative HV, with a current-mode anode output. It is shown in Figure 8.

Figure 8. LAMPF "Paint Can" beam loss monitor, and NE-4552 side-window photomultiplier. . The photomultiplier, mounted inside the can, is immersed in mineral-oil liquid scintillator.

The calibration is approximately 1000 μC per rad, including factors of 250 eV of energy loss per detectable photon, 3% collection efficiency, and 20% conversion efficiency.

$$1rad = \frac{100\,ergs}{gram} \cdot 350\,grams \cdot \frac{1eV}{1.6 \cdot 10^{-12} ergs} \cdot \frac{1\,photon}{250\,eV} = 9 \cdot 10^{13}\,photons;$$

$$9 \cdot 10^{13}\,photons \cdot 0.03 \cdot 0.2 \cdot 10{,}000\,gain \cdot \frac{1.6 \cdot 10^{-19} C}{electron} = 1000\,\mu C \qquad (9)$$

Thus the units are very sensitive, relative to ionization chambers. On the downside, there is a large unit-to-unit gain variation, a large sensitivity to voltage setting, and the mineral-oil scintillator eventually turns milky and must be replaced.

The LEDA CsI(Tl) Beam Loss Monitor

The LEDA beam loss monitor is designed with a very high radiation sensitivity in order to detect beam loses from a 6,7 MeV proton beam[13]. It is a commercially-packaged 5-cm dia. By 1.25-cm high CsI(Tl) crystal (110 grams) epoxied to an end-window photomultiplier. It is shown in Figure 9. The calibration is 1 uA output for a 190 mrad/hr source, equivalent to about 19,000 μC per rad.

$$1rad = \frac{100\,ergs}{gram} 110\,grams \frac{1eV}{1.6 \cdot 10^{-12} ergs} \frac{1\,photon}{15\,eV} = 4.6 \cdot 10^{14}\,photons$$

$$4.6 \cdot 10^{14}\,photons \cdot 0.6 \cdot 0.2 \cdot 2{,}150\,gain \cdot \frac{1.6 \cdot 10^{-19} C}{electron} = 19{,}000\ \mu C \qquad (10)$$

Gain curves for a few units are shown in Figure 10. Note that unlike ionization chambers, the sensitivity varies widely from unit to unit, as well as with the high voltage setting. However, the sensitivities are typically 10,000 to 500,000 times higher than ionization chambers.

Figure 9. The LEDA CsI(Tl) beam loss monitor. The calibration is about 19,000 μC per rad.

Figure 10. Gain curves for 8 LEDA beam loss monitors, at an exposure rate of 190 mrad/hr. The line at 1 μA is the calibration set point.

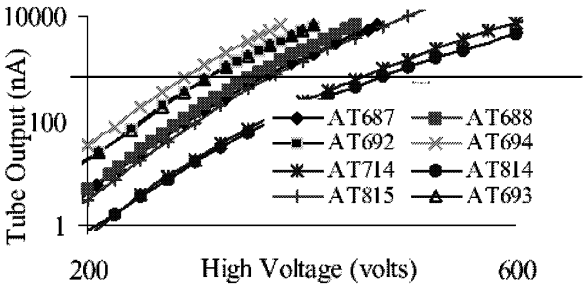

Scintillating Fibers and Optical Fibers

From time to time, scintillating fibers are suggested as a possible beam loss monitor. An interesting suggestion is to use Ce-activated Li glass (with Li^6) to detect neutrons. In general, the internal reflections and resultant attenuation are excessive unless a graded or stepped index fiber is used. A wavelength shifter must be used to limit self-absorption. For light produced isotropically in the fiber, only about 2% is in the cone that will be internally reflected. Lastly, the volume of the fiber is too small to produce sufficient light for most applications. Radiation darkening will probably limit the use to < 100 Mrad.

Cerenkov Radiators

Cerenkov light is the light emitted when a charged particle's velocity βc is greater then the light velocity c/*n* in a media with an index of refraction $n>1$. Specifically, the

number of photons N in an energy range ΔE eV emitted per cm in a Cerenkov radiator is[14]:

$$N = 369.8\left(1 - \frac{1}{n^2\beta^2}\right)\cdot \Delta E \ \ photons/cm \tag{11}$$

Cerenkov light is instantaneous, unlike scintillators, and the threshold for light output (β>1/n) is above Compton-electron energies of several hundred keV, making Cerenkov detectors useful where there is background radiation from RF cavity X-rays or synchrotron radiation, such as high-energy electron rings and superconducting RF cavities. For a 1-GeV proton (β=.875), a fused silica radiator (n =1.55), and photons between 400 and 600 nm, (ΔE = 1 eV), the light output is 169 photons per cm. It is emitted in a forward cone of half-angle $\cos^{-1}(1/n\beta)$. Figure 11 shows the photon yield vs particle energy (in mass units). Compton electrons below about 150 keV will not produce any light, while 1-GeV protons or 0.5 MeV electrons produce about 169 photons/cm.

The sensitivity is much less than phototube-scintillator combinations, however. For a 5-cm diameter, 1-cm thick fused-silica radiator, a collection efficiency of 80% and a cathode efficiency of 20%, a typical response to 1-GeV protons would be

$$1\,rad = \frac{3.1\cdot 10^7\, MIPs}{cm^2}\cdot 19.6\, cm^2 \cdot \frac{169\ photons}{MIP\ cm}\cdot 1\, cm\ thick = 1\cdot 10^{11}\ photons$$

$$1\cdot 10^{11}\ photons \cdot 0.8\cdot 0.2\cdot 10{,}000\ gain \cdot \frac{1.6\cdot 10^{-19} C}{electron} = 30\,\mu C \tag{12}$$

Figure 11. Plot of photons/cm vs. particle energy (in mass units) for three Cerenkov radiators:

Fused silica (n=1.55)
Water (n=1.33)
FC-75 (n=1.275)

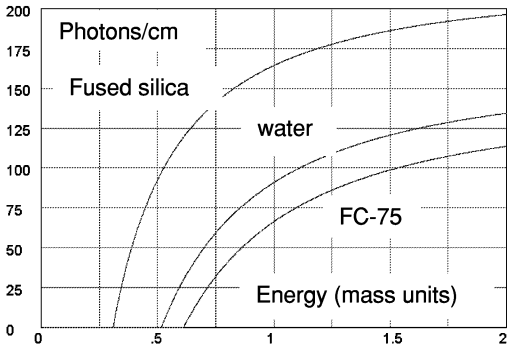

Ionizing Radiation Backgrounds

The most common background ionizing radiation around beam loss monitors is due to RF cavity x-rays (especially from superconducting cavities). Dark-current (x-ray) radiation around copper accelerator structures can be up to 50 rads/hr. The radiation spectrum from superconducting RF cavities can extend up into the MeV region.

Another source of ionizing radiation is synchrotron radiation from electron rings. A plot of the synchrotron radiation critical photon energy is shown in Figure 12. Unlike dark-current radiation from RF cavities, synchrotron radiation is very directional, so its effects can be minimized by proper beam loss monitor placement.

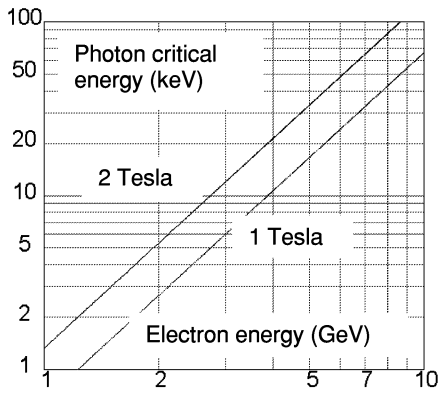

Figure 12. Synchrotron radiation critical photon energies in 1-Tesla and 2-Tesla magnetic fields, as a function of the electron energy.

In both cases, most of the radiation is sufficiently low energy so that it can be effectively shielded by high-*Z* material, such as lead. Tables of photon attenuation lengths are on the NIST website[1].

SUMMARY

The most widely used beam loss monitors are either of the current-integrating ionization-chamber design or the current-integrating photomultiplier-scintillator design. Both types produce a very wide dynamic range response. The phototube-scintillator combination has about a factor of 10,000 higher sensitivity to beam loss than ion chambers, but suffers from nonuniformity in unit-to-unit gains, and is very sensitive to voltage drifts.

Although ion chambers normally have poor time resolution compared to phototube-scintillator designs because of the slow electron drift velocities, special ion chamber designs using coaxial cable can achieve time resolutions of a few 10's of nsec.

In situations where there is low-energy background ionizing radiation (synchrotron radiation or RF cavity x-rays), phototube-Cerenkov radiators or PIN-diode pulse-coincidence circuits can be used. The latter are limited to a few rads/sec peak dose rates. Lead shielding can be used around any beam loss monitor to reduce the sensitivity to background x-rays.

REFERENCES

1. NIST website Physics.nist.gov. This website has tables of dE/dx and range for protons, as well as tables for photon cross sections.
2. Knoll, G.F., *Radiation Detection and Measurement* (Third Edition), Wiley,2000. See Table 5.1. This is a very good reference on radiation measurement instrumentation in general.
3. Boag, J.W., "Ionization Chambers", in *The Dosimetry of Ionizing Radiation*, Vol. **2**, Kase, K.R, Bjarngard, B.E., and Attix, F.H., Editors (Academic Press, 1987).
4. Boag J.W. and Wilson,T; *British Journal of Applied Physics* vol **3**, pages 222-229 (1952). See pages 226-227.
5. Shafer,R.E et al., The Tevatron BPM and BLM Systems, in *the Proceedings of the XII International Conference on High Energy Accelerators*, page 609 (Fermilab ,1983).
6. Reference 3, See Eqn (23) for charge collection efficiencies for continuous dose rates in cylindrical ion chambers, and Eqn (33) for charge collection efficiencies for pulsed doses in cylindrical ion

chambers, in chapter 3. This is an important reference for anyone designing an ion chamber for high dose rates.
7. Panofsky,W.K.H., SLAC Internal Tech Note TN-63-57 (1963).
8. McCormick, D., *Proceedings of the 1991 Particle Accelerator Conference*, pages 1240-42 (1991).
9. Ross, M.C. and McCormick, D. *Proceedings of the 1998 Linac Conference*, pages 192-194 (1998).
10. Wittenburg, K., in *Beam Instrumentation Workshop 2000*, pages 3-17 (AIP Conference Proceedings #546).
11. Website www.bergoz.com.
12. Reference 2, pages 226 and 235.
13. Sellyey W.C. et al., *Proceedings of the 2001 Particle Accelerator Conference*, pages 1315-1317 (2001)
14. Schiff L.I., *Quantum Mechanics* (Second Edition) McGraw Hill (1955). See Eqn(37.14) on page 271.